

Development and Application of a Multidimensional Database for the Detection of Quaternary Ammonium Compounds and Their Phase I Hepatic Metabolites in Humans

Ryan Nguyen, Ryan P. Seguin, Dylan H. Ross, Pengyu Chen, Sean Richardson, Jennifer Liem, Yvonne S. Lin, and Libin Xu*



Cite This: <https://doi.org/10.1021/acs.est.3c10845>



Read Online

ACCESS |



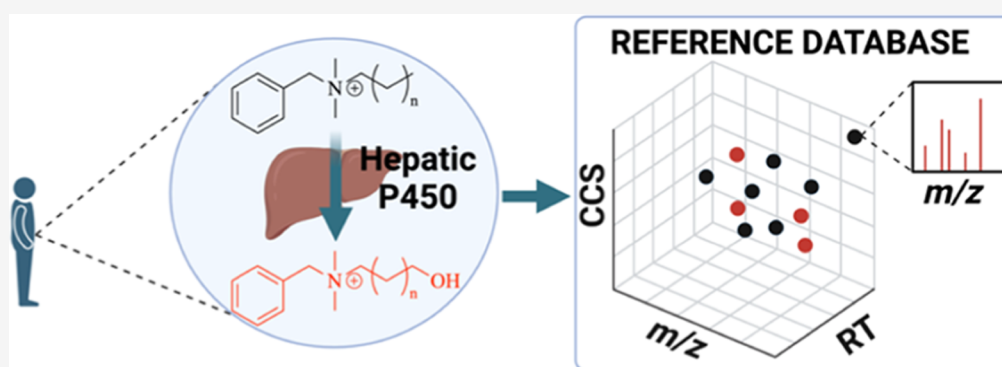
Metrics & More



Article Recommendations



Supporting Information



ABSTRACT: The COVID-19 pandemic has led to significantly increased human exposure to the widely used disinfectants quaternary ammonium compounds (QACs). Xenobiotic metabolism serves a critical role in the clearance of environmental molecules, yet limited data are available on the routes of QAC metabolism or metabolite levels in humans. To address this gap and to advance QAC biomonitoring capabilities, we analyzed 19 commonly used QACs and their phase I metabolites by liquid chromatography–ion mobility–tandem mass spectrometry (LC–IM–MS/MS). In vitro generation of QAC metabolites by human liver microsomes produced a series of oxidized metabolites, with metabolism generally occurring on the alkyl chain group, as supported by MS/MS fragmentation. Discernible trends were observed in the gas-phase IM behavior of QAC metabolites, which, despite their increased mass, displayed smaller collision cross-section (CCS) values than those of their respective parent compounds. We then constructed a multidimensional reference SQLite database consisting of m/z , CCS, retention time (rt), and MS/MS spectra for 19 parent QACs and 81 QAC metabolites. Using this database, we confidently identified 13 parent QACs and 35 metabolites in de-identified human fecal samples. This is the first study to integrate in vitro metabolite biosynthesis with LC–IM–MS/MS for the simultaneous monitoring of parent QACs and their metabolites in humans.

KEYWORDS: quaternary ammonium compounds (QACs), disinfectants, xenobiotic metabolism, ion mobility–mass spectrometry (IM–MS), biomonitoring, database, COVID-19

INTRODUCTION

Quaternary ammonium compounds (QACs) (Figure 1) are cationic surfactants with varying alkyl chain lengths (i.e., C_8 – C_{18}) that exhibit broad-spectrum antimicrobial properties.¹

QACs are relatively stable in the environment¹ and have been detected in numerous settings, including wastewater effluent,^{2–4} sludge,^{5,6} indoor dust,^{7,8} and food.^{9–11} Humans are chronically exposed to QACs due to their ubiquitous presence in cleaning solutions, medical products, and personal care goods and their use in the food-processing industry. Recent studies have revealed that QACs can be detected in virtually all human blood samples. Our previous analysis of 43 human blood samples collected pre-pandemic revealed that over 80% contained detectable levels of QACs (10–150 nM).¹² The

COVID-19 pandemic has led to elevated usage of QAC-containing disinfectants, and Zheng et al. reported that median QAC levels in human blood have increased by 77% since the start of the COVID-19 pandemic.¹³ Furthermore, QACs have been detected in human breast milk, suggesting that nursing infants may potentially be exposed to these compounds.¹⁴

Received: December 22, 2023

Revised: March 6, 2024

Accepted: March 8, 2024

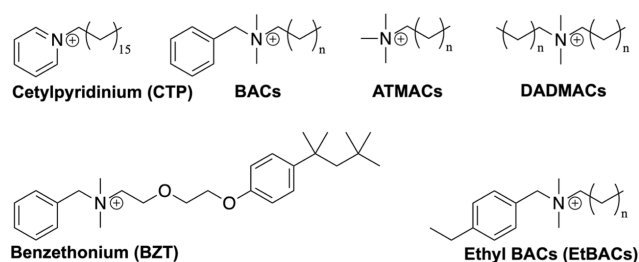


Figure 1. Chemical structures of commonly used quaternary ammonium compounds (QACs): cetylpyridinium (CTP), benzalkonium compounds (BACs), alkyltrimethylammonium compounds (ATMACs), dialkyldimethylammonium compounds (DADMACs), benzethonium (BZT), and ethylbenzalkonium compounds (EtBACs). The QACs investigated herein contain even-numbered alkyl chain lengths that range from C₈ to C₁₈.

These studies suggest that there is a high prevalence of chronic exposure to QACs, especially as the COVID-19 pandemic amplified the habitual use of disinfectants.

Concerns about QAC toxicity have increased in recent years. The FDA has requested additional safety information on the usage of benzalkonium compounds (BACs), a subgroup of QACs commonly found in consumer and medical antiseptic products.^{15,16} Last year, the Toxics Use Reduction Institute (TURI) at the University of Massachusetts in Lowell recommended that certain BACs and dialkyldimethylammonium compounds (DADMACs) be added to the Toxic Use Reduction Act List of Hazardous Substances, citing their associations with acute and chronic health effects.¹⁷ Both BACs and DADMACs have been shown to disrupt mitochondrial function^{18,19} and exacerbate inflammation *in vitro*,¹² and we previously demonstrated that short-chain BACs potently inhibit 7-dehydrocholesterol reductase (DHCR7), the last enzyme in mammalian cholesterol biosynthesis.²⁰ Alkyltrimethylammonium compounds (ATMACs), a group of QACs commonly found in fabric softeners and hair conditioners, are highly toxic to aquatic organisms.²¹ Furthermore, depressed skeletal muscle contractility was observed in female rats that had sublethal intravenous injections of C₁₂–C₁₄ alkyltrimethylammonium bromides administered to them.²² Respiratory effects have also been reported in animal studies. Mice exposed to various aerosolized QACs, for example, had reduced lung tidal volume and pulmonary inflammation.²³ Melin et al. demonstrated that chronic BAC consumption (60 or 120 mg/kg/day) led to significantly decreased fertility and fecundity in mice.²⁴ Furthermore, QAC exposure in humans has been associated with allergic-contact dermatitis,²⁵ work-related asthma,²⁶ and increased risk of chronic obstructive pulmonary disease.²⁷

Despite the high prevalence of chronic exposure to QACs among human populations and the wide range of reported QAC toxicities, there is a major gap in knowledge regarding the metabolism of these compounds in mammalian species. Metabolism determines the fate of xenobiotic substances in the body and their potential to cause adverse effects, primarily through detoxification or bioactivation. Indeed, we previously demonstrated that cytochrome P450 (CYP)-mediated metabolism of C₁₀-BAC mitigates its inhibition of DHCR7.²⁸ This finding suggests that metabolism is involved in regulating the toxicity of QACs, yet, to date, biomonitoring studies of these compounds have neglected to detect or report QAC metabolite levels in humans.

To confidently detect and identify QAC metabolites in human samples at the scale necessary for biomonitoring studies, new analytical methods that are both rapid and scalable must first be developed. We therefore developed a novel analytical workflow based on ion mobility–mass spectrometry (IM–MS).^{29,30} In this technique, gas-phase analytes are rapidly separated depending on their size and shape as they are driven through a neutral buffer gas (such as N₂) under the influence of a static (i.e., drift-tube IM, DTIM) or dynamic electric field (i.e., traveling wave IM, TWIM). Ions with a smaller rotationally averaged surface area or collision cross-section (CCS) exhibit greater mobility within the drift tube (and therefore shorter drift times) than less structurally compact gas-phase ions. IM–MS consequently enables three-dimensional separation when coupled to polarity-based liquid chromatography–tandem mass spectrometry (LC–MS/MS). Unlike retention time (*rt*) values, CCS measurements are not affected by differences in mobile phase composition, analytical column type, or gradient method. While the reproducibility of interday and interlaboratory ^{TWIM}CCS measurements is high (<1.5% relative standard deviation) for analyte classes such as steroids,³¹ mycotoxins,³² drugs,³⁰ and drug-like compounds,³⁰ external calibrants are necessary to obtain CCS measurements from drift times measured in TWIM due to the non-uniform nature of the applied electric field. Although a small number of large errors between some CCS values acquired on DTIM and TWIM have been reported, the errors for the majority of the data are less than 3%,^{33,34,45} including environmental chemicals and their metabolites.³⁴ The identification of small organic molecules in complex mixtures using IM–MS analytical workflows is, therefore, feasible with appropriate CCS tolerances, as we have shown in our previous work.³⁵

To facilitate the detection and identification of QACs and their metabolites with potential toxicological significance in human biomonitoring studies, we developed the first reference ^{TWIM}CCS_{N₂} database, encompassing 19 commonly used QACs and their 81 detected phase I hepatic metabolites. We utilized two widely accepted sets of CCS calibrants [poly-DL-alanines,³⁰ PolyAla, and a mixture of hexakis(fluoroalkoxy)-phosphazenes,³⁶ HFAPs], as well as a custom mixture of drug and drug-like CCS calibrants,³⁰ to increase the accessibility of our reference database across platforms. To position the metabolite CCS as an orthogonal identifier in a high-throughput metabolite identification workflow, we coupled *in vitro* metabolite biosynthesis to LC–IM–MS analysis and developed open-source software tools for post-acquisition data processing and visualization. A second reference database containing post-IM–MS/MS fragmentation spectra was also collected to further investigate metabolite structures and to improve the confidence of peak annotations via MS/MS cosine similarity scoring of fragmentation spectra. To demonstrate the feasibility of integrating LC–IM–MS workflows into human biomonitoring studies, we analyzed de-identified human fecal samples (*n* = 5) for QACs and their metabolites using our CCS reference database.

■ MATERIALS AND METHODS

Materials. Optima LC/MS grade acetonitrile, methanol, water, formic acid, and ammonium formate were purchased from Fisher Scientific (Pittsburgh, PA). The following chemicals were purchased from Sigma-Aldrich (St. Louis, MO): molecular biology-grade dimethyl sulfoxide (DMSO), poly-DL-alanine, acetaminophen (≥98% purity), betaine hydro-

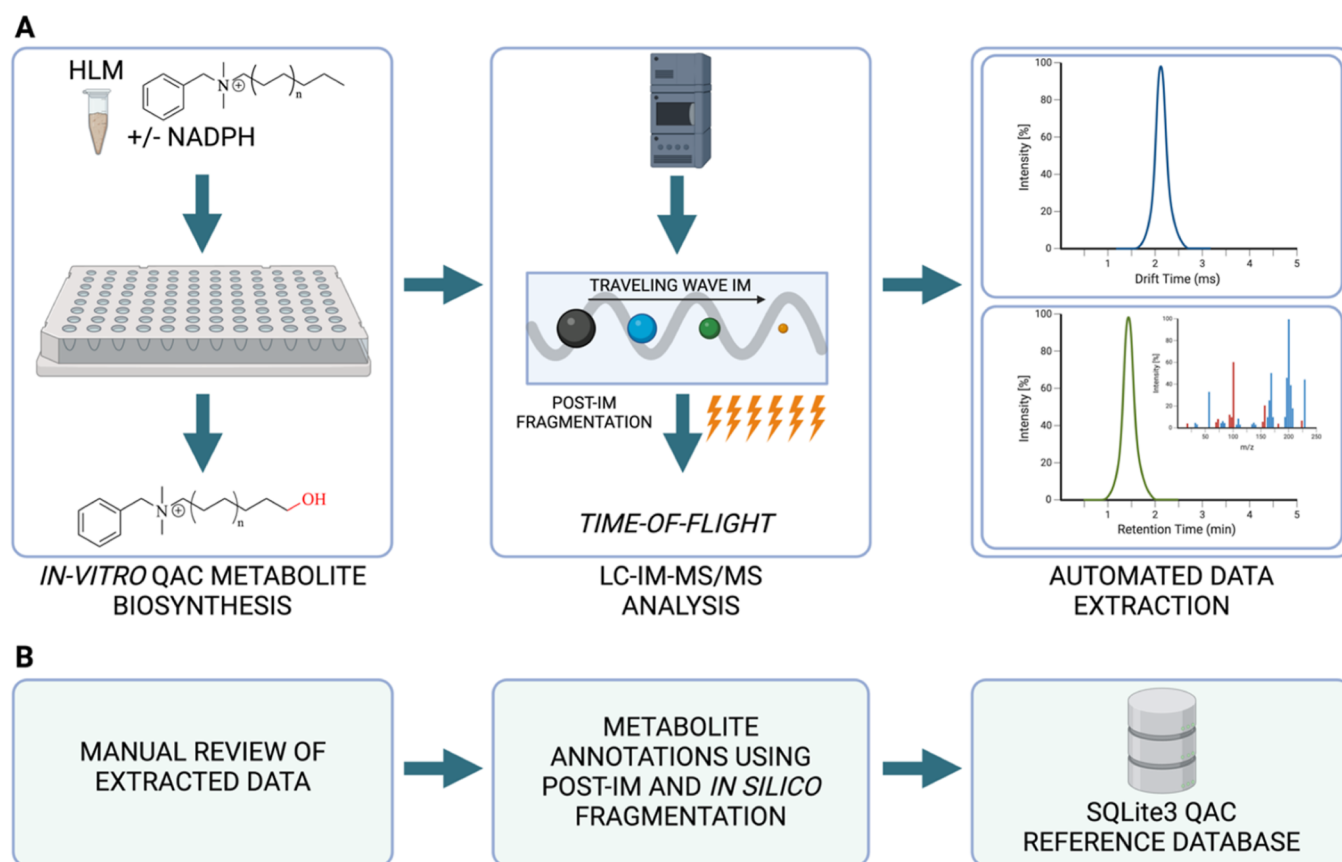


Figure 2. Overview of the experimental workflow for constructing the QAC reference database. (A) QAC metabolites were generated in NADPH-supplemented HLM and subsequently analyzed via LC–IM–MS/MS analysis with automated data extraction. (B) Data were manually reviewed and annotated to compile a custom SQLite reference database encompassing parent QACs and their observed phase I hepatic metabolites.

chloride ($\geq 98\%$ purity), ATMACs (C_8 – C_{18}), BACs (C_8 – C_{18}), ethyl BACs (EtBACs; as a mixture of C_{12} and C_{14}), DADMACs (C_{10} – C_{16}), benzethonium chloride (BZT), and cetylpyridinium chloride (CTP) ($\geq 97\%$ purity). Alprenolol hydrochloride, clozapine N-oxide, ondansetron, reserpine, verapamil, and vancomycin were purchased from Cayman Chemical (Ann Arbor, MI) with a purity of $\geq 98\%$. A mixture of hexakis(fluoroalkoxy)phosphasphazines (HFAPs; ESI-L low-concentration tuning mix) was purchased from Agilent Technologies (Santa Clara, CA). Pooled human liver microsomes (HLM) from 20 liver donors (10 males/10 females) were purchased from XenoTech, LLC (Kansas City, KS). Nicotinamide adenine dinucleotide phosphate (NADPH) cofactor was purchased from Oriental Yeast (Tokyo, Japan).

Poly-DL-alanine was prepared at 25 $\mu\text{g}/\text{mL}$ in 1:1 acetonitrile/water with 0.1% formic acid. A mixture of drug and drug-like compounds containing acetaminophen (10 μM), betaine (10 μM), alprenolol (2 μM), clozapine N-oxide (2 μM), ondansetron (2 μM), reserpine (2 μM), verapamil (2 μM), and vancomycin (2 μM) was prepared in 1:1 acetonitrile/water with 0.1% formic acid. The ESI-L low-concentration tuning mix was prepared by 1:4 dilution in 95% acetonitrile in water. All QACs were diluted in DMSO to 10 mM, except for the ethyl BACs that were diluted to 5 mg/mL in DMSO.

In Vitro QAC Metabolite Biosynthesis. QAC metabolites were generated in vitro using pooled HLM in a 96-well plate format following a protocol from our previous work.^{29,35} First, the HLM stock (20 mg/mL protein) was thawed on ice

and diluted with a buffer (0.1 M potassium phosphate, KPi at pH 7.4) followed by the addition of a substrate from concentrated DMSO stock (QAC at 10 mM; exceptions were C_{18} -DADMAC and C_{12}/C_{14} -EtBACs, which were prepared at 2 and 5 mg/mL, respectively). The mixtures were distributed across 4 wells (180 $\mu\text{L}/\text{well}$) into a 96-well plate resting on ice. The plate was then transferred to a 37 $^{\circ}\text{C}$ water bath and equilibrated for 3 min before the first of the 4 wells was initiated with 20 μL of KPi buffer (-NADPH negative control). The second, third, and fourth wells were initiated with 20 μL of NADPH (10 mM in KPi buffer). The formation of known NADPH-dependent BAC metabolites²⁸ (Figure S1), which served as positive controls, was manually confirmed. All incubations were performed at final concentrations of 0.5 mg/mL HLM protein and 50 μM substrate, except for the EtBACs, which were incubated at a substrate concentration of 25 $\mu\text{g}/\text{mL}$ because they are sold as a mixture of C_{12} and C_{14} -EtBACs. The percentage of DMSO (v/v) in the incubations was $\leq 0.5\%$. For C_8 – C_{18} -ATMACs, C_8 – C_{12} -BACs, and CTP, incubations were quenched after 15 and 30 min by addition of 1 volume equivalent of ice-cold acetonitrile. For the remaining compounds, incubations were quenched in the same manner after 40 and 80 min. All quenched reactions were rested on ice for 10 min to facilitate protein precipitation and centrifuged (4000 rpm, 4 $^{\circ}\text{C}$, 15 min). Finally, the supernatant was transferred to a fresh 96-well plate and diluted 1:2 into a 2:1 mixture of water/methanol for subsequent LC–IM–MS/MS analysis.

LC–IM–MS/MS Analysis of Human Liver Microsome QAC Incubations. HLM incubation samples (5 μL) were injected and separated with a Waters Acquity UPLC, which was equipped with a quaternary solvent pump and a refrigerated autosampler (10 $^{\circ}\text{C}$) coupled to a reversed-phase Phenomenex Kinetex C_8 column (100 \times 2.1 mm, 1.7 μm particle size). Due to the wide range of log K_{ow} values for the selected compounds and their metabolites, we employed 4 chromatographic gradients consisting of varying compositions of solvent A (0.1% formic acid, 2 mM ammonium formate in water) and solvent B (acetonitrile) at a flow rate of 0.4 mL/min, as outlined in Table S1. The eluted analytes were detected in full-scan IM-MS mode over the range of 50–1200 m/z on a Waters Synapt XS Q-TOF mass spectrometer (Waters Corp., Milford, MA) using nitrogen as the drift gas. The ESI(+) conditions were set at a source temperature of 150 $^{\circ}\text{C}$ and a capillary voltage of 2.5 kV. Additional source parameters were as follows: de-solvation temperature, 500 $^{\circ}\text{C}$; cone gas flow, 50 L/h; nebulizer gas flow, 6.5 bar; desolvation gas flow, 1000 L/h; cone voltage, 30 V; and source offset, 10 V. The mass analyzer was calibrated using sodium formate over the range of 50–1200 m/z in “resolution” mode. IM separations were achieved at a traveling wave velocity of 500 m/s and a height of 40 V. For post-IM fragmentation, a ramp from 25 to 45 V was added to the transfer region. A leucine-enkephalin lock mass ($[\text{M} + \text{H}]^+ = 556.2771$ m/z) was applied as a mass correction reference during data acquisition. Each set of CCS calibrants (PolyAla, HFAPs, and the drug/drug-like mixture) was analyzed at the beginning and end of each plate analysis using flow injection analysis (FIA) consisting of 10 μL injections and a 0.4 mL/min flow of 95% water with 0.1% formic acid/5% acetonitrile. Calibrant data were acquired for 1 min with a 0.5 s scan time over the range of 50–1200 m/z . The 96-well plates containing incubation extracts were analyzed on two separate occasions over 9 months, with multiple injections of technical replicates on each occasion, to assess intraday and interday variability.

TWIM CCS Calibration. To calibrate TWIM drift times (dt) into $^{\text{TWIM}}\text{CCS}_{\text{N}_2}$ values, we used the reference nitrogen drift tube CCS values ($^{\text{DT}}\text{CCS}_{\text{N}_2}$) of a series of singly charged poly-DL-alanines³⁰ ($n = 2$ –14), a custom mixture of drug and drug-like compounds³⁰ ($n = 7$), and a mixture of HFAPs from the Agilent ESI-L low-concentration tuning mix³⁶ ($n = 4$), as we have previously described.^{29,30} First, custom Python scripts were used to automatically extract mobilograms for CCS calibrants from the raw data using an accurate mass window of ± 0.01 Da. For each calibrant, drift times were calculated as the mean from a least-squares fit of a Gaussian function on the raw mobilogram and corrected for mass-dependent flight time to obtain corrected drift times (t'_d). Reference CCS values were also corrected for the ion charge state and reduced mass with the drift gas to obtain corrected CCS values (CCS'). A CCS calibration curve of the form $\text{CCS}' = A(t'_d + t_0)^B$, where A , t_0 , and B are fit parameters, was generated from the reference data for each set of calibrants and manually inspected. Calibration curves displaying randomly distributed fit residuals with a maximal error of $<3\%$ were considered acceptable (Figure S2).

LC–IM–MS/MS Data Processing. We adapted our previously described IM–MS analytical workflow³⁵ to extract the retention times, CCS values, and MS/MS fragmentation spectra for QACs and their metabolites (Figure 2).

Data processing was performed by using custom Python scripts freely available on GitHub. First, target lists containing

the path to a raw data file, exact m/z , and the putative compound name for known parent QACs and their expected phase I metabolites were assembled to automatically extract m/z -selected mobilograms from the raw data with a mass tolerance of ± 0.025 Da. Only $[\text{M}]^+$ ions were included in the current study. The mobilograms were fit with a Gaussian function to obtain drift times, which were converted to calibrated CCS values by applying the CCS calibration curves described above. All extracted mobilograms were manually inspected for intensity (>1000), peak width (full width at half-maximum between 0.06 and 1.77 ms), and quality of the Gaussian fit (i.e., multimodality). Ions with mobilograms that did not meet these empirical cut-offs were flagged and not processed further. The drift times of the accepted mobilograms were appended to the original target lists to automatically extract m/z - and dt -selected LC ion chromatograms for parent QACs and their observed metabolites. Retention time (rt) for the peaks in the extracted LC ion chromatograms was detected using the “find_peaks” function in SciPy (version 1.8.1).³⁷ The NADPH-dependence of all observed metabolites was manually confirmed by comparing the extracted LC ion chromatograms of control ($-\text{NADPH}$) incubations to those of experimental ($+\text{NADPH}$) incubations (Figure S3). Finally, rt - and dt -selected post-IM fragmentation spectra for parent QACs and their NADPH-dependent metabolites were automatically extracted from the raw data and scored against in silico fragmentation spectra generated with MS-Finder³⁸ (version 3.52) (Figure S4). Fragmentation spectra with a total score (representing a combined weighting score that accounts for mass accuracies, fragment linkages, hydrogen rearrangement rules, and bond dissociation energies) of >5 out of 10 were considered acceptable.

Development of a QAC and Metabolite Reference Database. We developed a custom SQLite database to store experimental data and associated metadata for parent QACs and the detected metabolites included in this study. The database was constructed in an automated fashion using custom Python scripts and contains a single table, called *qacs_rt_ccs*, with the following columns: *compound_name*, *exact_mz*, *rt*, *average_ccs*, *ccs_calibrant*, *gradient*, *column_type*, and *notes*. As discussed above, the CCS values and retention times from the LC–IM–MS/MS analyses were automatically extracted from the raw data and manually reviewed. The CCS value reported for each parent QAC and metabolite in the database represents the average measurement ($n = 3$ –6) of biological replicates (i.e., independent + NADPH reaction mixtures). For each compound, the average CCS value was calculated after identifying and removing outliers, which were defined as observations falling outside 1.5 times the interquartile range. Replicates displaying relative standard deviations (RSDs) below 1.5% were considered acceptable for inclusion in the database on the basis that similar RSDs have been reported for $^{\text{TWIM}}\text{CCS}_{\text{N}_2}$ values measured on the same instrument over time.³¹ The total number of measurements used to calculate the average CCS value for each compound as well as the associated time points for each reaction mixture and observed relative standard deviations are reported in the Supporting Information. Metabolite annotations were validated for NADPH-dependence and similarity to the in silico fragmentation spectra. The database was first initialized with the empty *qacs_rt_ccs* table, and the experimental data and associated metadata were added to the table. Two additional databases were initialized to store the

experimental (i.e., previously collected) and theoretical (i.e., in silico) *rt*- and *dt*-selected post-IM fragmentation spectra for the parent QACs and their observed metabolites. The experimental and theoretical MS/MS databases contain a single table, called *experimental_msms_data* and *theoretical_msms_data*, respectively, with the following columns: *compound_name*, *mz*, and *normalized_intensity*. Fragmentation spectra for the experimental MS/MS database were extracted from the raw data as described above and normalized to the most intense *m/z* peak. For the theoretical MS/MS database, in silico fragmentation spectra were generated with MS-Finder and then automatically extracted from the output text files by using a custom Python script.

Human Fecal Sample Collection. Healthy volunteers between the ages of 18 and 49 years with a BMI between 18 and 27 kg/m² were recruited for a study to collect fecal, urine, and blood samples. The study was approved by the University of Washington Institutional Review Board. Study participants completed an online screening questionnaire with the following exclusion criteria: diagnosis of any significant medical conditions, including cardiac, hepatic, gastrointestinal, renal, or autoimmune disease, diabetes, or other metabolic diseases; taking medication or supplements within the last 2 weeks that might affect cholesterol or lipid levels; or currently pregnant or breast-feeding. Following online consent, participants were given a commercially available fecal collection kit (Easy-Sampler Stool Collection Kit, ALPCO, Salem, NH). Participants were instructed to collect fecal samples within 24 h of a scheduled visit, aliquot fecal samples into 4 screw-top tubes (~2 mL per tube), and store their samples in provided sealable bags in their freezers before their scheduled visit. Upon receipt of the fecal samples, samples were stored at -80 °C until analysis.

Preparation of Human Fecal Samples. Aliquots of ice-cold human fecal samples (50 mg wet weight, *n* = 5) were weighed into Eppendorf tubes and immediately treated with 200 μL of ice-cold 3:1 water/ethanol. The samples were vortexed and sonicated on ice for 30 min. Next, 20 μL of acetonitrile containing a mixture of deuterated (*d*₇-benzyl) BACs as internal standards (10 pmol each of *d*₇-C₁₀-C₁₆ BACs and *d*₀-C₆-BAC, which is not commercially produced) was added to each sample, followed by continuous vortexing for 5 min. An additional 750 μL of pure acetonitrile was added, and the samples were vortexed for 20 min before being centrifuged at 16,000*g* for 10 min at ambient temperature. After centrifugation, 750 μL of the supernatant from each sample was transferred to glass vials. The remaining pellet from each sample was re-suspended in 750 μL of 9:1 methanol/chloroform, followed by centrifugation at 16,000*g* for 10 min at ambient temperature. The two supernatants were combined in glass vials and evaporated overnight in a chemical fume hood. After evaporation, the residue from each sample was reconstituted in 500 μL of 4:1 acetonitrile/water, transferred to 0.22 μm spin filter tubes, and centrifuged at 16,000*g* for 5 min. Finally, the filtrate from each sample was transferred to glass LC vials for subsequent LC-IM-MS/MS analysis. Blank water controls (extraction of 50 μL of H₂O in place of 50 mg of feces) were also prepared alongside the fecal samples using an identical procedure. To demonstrate our analytical workflow, we began by pooling the 5 human fecal extracts (50 μL each) and analyzed the sample via LC-IM-MS/MS (see below). The five individual human fecal samples were subsequently analyzed using the same procedures.

LC-IM-MS/MS Analysis of Human Fecal Samples.

Human fecal extracts (5 μL) were injected and separated with a Waters Acquity UPLC coupled to a reversed-phased Phenomenex Kinetex C₈ column (100 × 2.1 mm, 1.7 μm particle size). Each sample was eluted with the four chromatographic gradients described above (LC-IM-MS/MS Analysis of Human Liver Microsome QAC Incubations). The eluted analytes were detected in full-scan IM-MS mode over the range of 50–1200 *m/z* on a Waters Synapt XS Q-TOF mass spectrometer (Waters Corp., Milford, MA) using nitrogen as the drift gas. The ESI(+) conditions were set at a source temperature of 110 °C and a capillary voltage of 2.5 kV. Additional source parameters were as follows: desolvation temperature, 200 °C; cone gas flow, 10 L/h; nebulizer gas flow, 5 bar; desolvation gas flow, 800 L/h; cone voltage, 30 V; and source offset, 10 V. The mass detector was calibrated using sodium formate over the range of 50–1200 *m/z* in “resolution” mode. IM separations were achieved at a traveling wave velocity of 500 m/s and a height of 40 V. For post-IM fragmentation, a ramp from 20 to 30 V was added to the transfer region. A leucine-enkephalin lock mass ([MH]⁺ = 556.2771 *m/z*) was applied as a mass correction reference during data acquisition. Each set of CCS calibrants (PolyAla, HFAPs, and the drug/drug-like mixture) was analyzed at the beginning of each plate analysis using flow injection analysis (FIA), as described above. Automated CCS calibration, peak picking of the raw data files, and subsequent queries against the QAC reference database were performed by using custom Python scripts. Briefly, a target list containing the exact *m/z* values of parent QACs and their observed phase I hepatic metabolites was compiled and used to extract *m/z*-selected LC ion chromatograms from the raw data files (±0.025 Da from theoretical values). Only [M]⁺ ions were included. The extracted LC chromatogram peaks were (1) automatically smoothed using Gaussian convolution, (2) picked, (3) fitted to a multi-Gaussian function, and (4) integrated to obtain peak areas before being applied to extract *m/z*- and *rt*-selected mobilograms from the raw data files (±0.1 min from the picked LC chromatogram peak). The extracted *m/z*- and *rt*-selected mobilograms were fitted to a Gaussian function to obtain drift times, which were converted to calibrated CCS values as described above (see TWIM CCS Calibration). This process generated a list of extracted spectral features, which was automatically compared against the spectral features extracted from a gradient-matched blank control to remove non-unique entries. Finally, the list of unique spectral features containing the exact *m/z* and *rt* LC ion chromatogram peak area and calibrated CCS value was queried against the QAC reference database using various selection criteria, including (1) *m/z*, (2) *m/z* and *rt*, (3) *m/z* and CCS, (4) *m/z*, *rt*, and CCS, and (5) *m/z*, *rt*, CCS, and MS/MS spectral cosine similarity to reference spectra. Search tolerances of 0.025 Da, 0.2 min, and 3% were applied for *m/z*, *rt*, and CCS, respectively. We previously demonstrated that these tolerance values generate highly reproducible and accurate lipid identifications in LC-IM-MS data sets.³⁹ All returned potential matches were manually investigated to confirm the peak shape, quality of fit, and presence of sufficient intensity above the blank control. Semiquantitation of C₁₀, C₁₂, C₁₄, and C₁₆-BAC concentrations identified in the human fecal extracts was performed using the peak area ratio of the corresponding internal standard (IS) *d*₇-labeled BAC⁴⁰

$$[\text{BAC}] = \frac{\text{peak area}_{\text{BAC}}}{\text{peak area}_{\text{IS}}} [\text{IS}]$$

This data processing workflow is summarized in Figure S5.

Code and Data Availability. All code for generating the QAC reference database and processing human samples is available on GitHub (https://github.com/libinxulab/xulab_software.git). Experimental fragmentation data and the associated SQLite database files are also available on GitHub for download. Raw mass spectrometry data are available at MassIVE under MSV000093621. The QAC reference database can also be queried on CCSbase.

RESULTS AND DISCUSSION

In Vitro QAC Metabolite Biosynthesis. A total of 19 commonly used QACs were incubated in NADPH-supplemented HLM. We identified NADPH-dependent mono- and dihydroxylated metabolites (+1O and +2O) (Figure S3), in addition to further oxidized and desaturated metabolites (+1O,-2H, +2O,-2H, and +3O,-2H), as summarized in Table 1.

Table 1. Summary of Observed QAC Microsomal Metabolites (✓, Observed; X, Not Observed)

	+1O	+2O	+1O,- 2H	+2O,- 2H	+3O,- 2H	- 2H	N- dealkylation
ATMAC							
C ₈	✓	✓	✓	X	✓	✓	X
C ₁₀	✓	✓	✓	✓	X	✓	X
C ₁₂	✓	✓	✓	✓	X	X	X
C ₁₄	✓	✓	✓	✓	X	X	X
C ₁₆	✓	✓	✓	✓	X	X	X
C ₁₈	✓	✓	✓	✓	X	X	X
DADMAC							
C ₁₀	✓	✓	✓	✓	✓	X	X
C ₁₂	✓	✓	✓	✓	✓	X	X
C ₁₄	✓	✓	✓	✓	✓	X	X
BAC							
C ₈	✓	✓	✓	✓	X	✓	X
C ₁₀	✓	✓	✓	✓	X	X	X
C ₁₂	✓	✓	✓	✓	X	X	X
C ₁₄	✓	✓	✓	✓	✓	X	X
C ₁₆	✓	✓	✓	✓	✓	X	X
C ₁₈	✓	✓	✓	✓	✓	X	X
EtBAC							
C ₁₂	✓	✓	✓	✓	✓	✓	X
C ₁₄	✓	✓	✓	✓	✓	X	X
BZT	✓	✓	✓	✓	✓	✓	X
CTP	✓	✓	✓	✓	X	✓	X

Metabolites were consistently detected across biological replicates and time points, with all metabolites present from the initial time point measured in the reaction (i.e., 15 or 40 min, see *In Vitro QAC Metabolite Biosynthesis*). Basic experimental data, including observed mass accuracies, retention times, detection frequencies, and characteristic fragments, are available in the *Supporting Information*.

For each ATMAC, we consistently observed two major +1O metabolite peaks in the LC chromatograms. A representative example of ATMAC metabolite characterization is shown in Figure 3A for C₁₀-ATMAC metabolite.

These findings suggest that ATMAC metabolism followed a similar pathway to that of BACs, which we have previously shown are oxidized exclusively along the alkyl chain region by cytochrome P450 (CYP) enzymes to *ω*-hydroxy (terminal) and (*ω*-1)-hydroxy metabolites.²⁸ As such, the observed sequential oxidation products in our microsomal ATMAC incubations are likely dihydroxy (+32 Da), ketones (+14 Da), and *ω*-carboxylic acid (COOH) (+30 Da) metabolites. We did not observe metabolite *m/z* values associated with N-dealkylation for any of the investigated QACs. Moreover, the presence of an intact trimethylamine fragment (60.084 observed *m/z*; 60.081 theoretical *m/z*) in the MS/MS fragmentation spectra of both the parent ATMACs and the observed ATMAC metabolites indicates that these oxidation and desaturation reactions occurred along the alkyl chain region (Figures 3B–F and 4).

Similar trends were observed for C₁₀-DADMAC, which appeared to form at least two major +1O- and +2O metabolites and multiple sequentially oxidized metabolites (+1O,-2H and +2O,-2H) (Figures S6 and S7). Additional +1O metabolites present in lower abundance were also observed, which suggests that oxidation could also occur at further internal carbon positions (e.g., *ω*-2, *ω*-3, etc.). Our data indicate that the second addition of oxygen to C₁₀-DADMAC occurred at various carbon positions, leading to dihydroxylation on a single alkyl chain (Figure S7C, C₁₂H₂₈NO⁺ fragment) or distributed across both alkyl chains (Figure S7D, C₁₂H₂₆NO₂⁺ fragment) for the dialkyl series of QAC substrates. Similarly, both C₁₂-EtBAC and C₁₄-EtBAC formed at least two structurally distinct NADPH-dependent +1O metabolites, leading to numerous +2O and further oxidized metabolites (Figures S8 and S9). In the extracted ion chromatogram of +1O-C₁₂-EtBAC, a metabolite eluting at 4.14 min displayed an unmodified ethylbenzyl cation fragment with an observed *m/z* of 119.088 (119.086 theoretical *m/z*), indicating that oxygen insertion occurred at the C₁₂ alkyl chain. For the metabolite eluting at 5.78 min, the ethylbenzyl cation contained a +16 Da modification with an observed *m/z* of 135.082 (135.081 theoretical *m/z*), indicating that oxygen insertion likely occurred on the ethylbenzyl group in this instance (Figure S9).

In addition to these oxygenated metabolites, we identified multiple desaturated (parent-2H) metabolites of BAC, EtBAC, ATMAC, CTP, and BZT without the addition of oxygen, suggesting that these QACs undergo atypical phase I metabolism (Figures S10–S12). In the case of BZT, chromatographic separation on the LC column resolved at least 6 unique BZT + O and 4 BZT-2H metabolite peaks (Figure S11A). Although it is plausible that BZT could undergo *O*-dealkylation at its ether linkages, we did not observe the expected *m/z* values associated with these reactions in our microsomal incubations. Moreover, the presence of an unmodified benzyl cation (91.056 observed *m/z*; 91.054 theoretical *m/z*) in the MS/MS fragmentation spectra of the parent BZT and its metabolites (Figure S11B–F) suggests that the observed modifications occur on the 2,4,4-trimethyl-pentan-2-yl (TMP) moiety. However, the lack of vicinal C–H groups on TMP precludes direct desaturation. The observed BZT-2H metabolites could therefore be alkene products that form after intramolecular rearrangement of TMP brings two C–H groups into vicinal positioning, as would be possible in a CYP-mediated methyl shift reaction. Additional mechanistic and structural studies of these novel metabolites

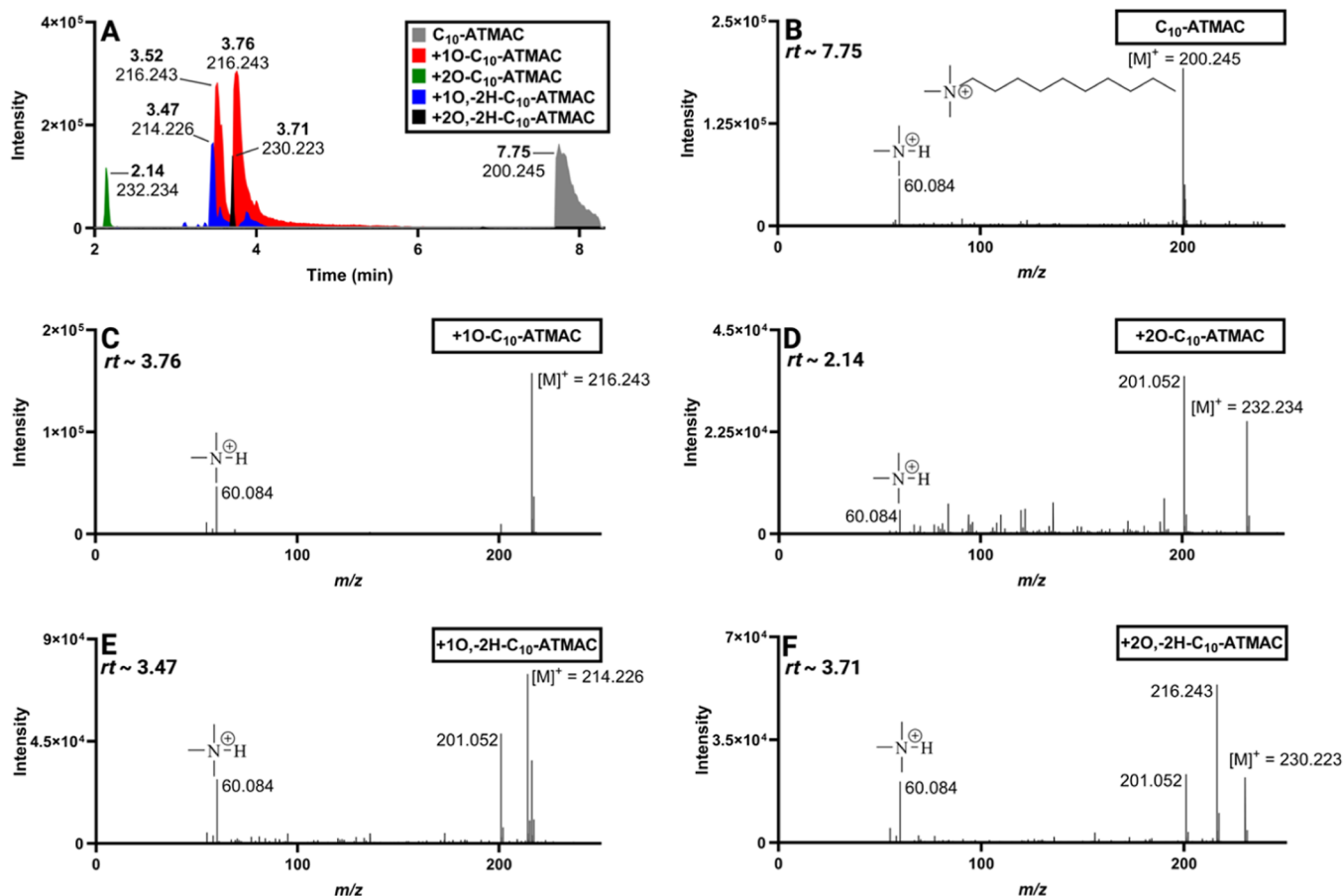


Figure 3. Identification of C_{10} -ATMAC microsomal metabolites. (A) LC-MS extracted ion chromatograms (± 0.025 Da from theoretical values) displaying parent (gray), monohydroxylated (red), dihydroxylated (green), and further oxidized (+1O,-2H and +2O,-2H) C_{10} -ATMAC metabolites (blue and black, respectively). Peaks are labeled with observed m/z values and retention times. MS/MS fragmentation spectra of (B) parent C_{10} -ATMAC, (C) +1O- C_{10} -ATMAC, (D) +2O- C_{10} -ATMAC, (E) +1O,-2H- C_{10} -ATMAC, and (F) +2O,-2H- C_{10} -ATMAC demonstrating the consistent loss and detection of a trimethylamine fragment (60.081 theoretical m/z).

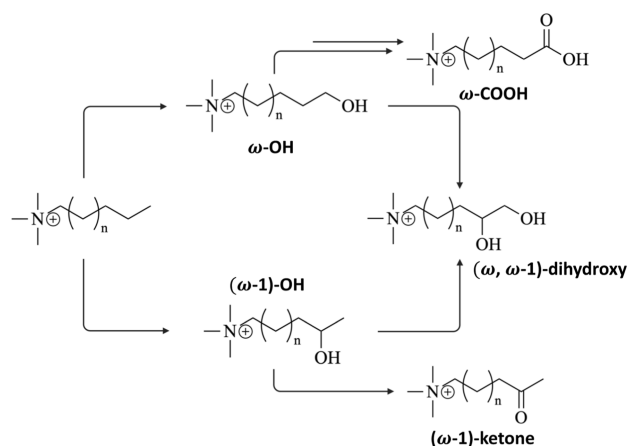


Figure 4. Summary of proposed ATMAC metabolism by NADPH-supplemented HLM. Metabolite structures are based on the consistent observation of two peaks in the LC-MS extracted ion chromatograms of +1O-ATMACs. Tentative assignment of the ω and $\omega-1$ oxidized carbon positions is based on our previously reported findings on BAC metabolism.²⁸

are ongoing. While these desaturated metabolites were relatively minor in comparison to the most abundant +1O oxygenated metabolites ($\sim 17\%$ relative peak area), they have the potential to be toxicologically relevant given the ability of

bioactivated alkenes to form adducts with cellular molecules.⁴¹ For example, the hepatotoxicity of valproic acid (VPA), an anticonvulsant drug used for the treatment of epilepsy, is a consequence of the CYP-mediated desaturation of VPA to a terminal alkene (Δ^4 -VPA).^{42,43} In addition to being a potent mechanism-based inhibitor of CYP enzymes, Δ^4 -VPA is a strong inducer of steatosis due to its disruption of fatty acid β -oxidation.⁴²

The detection of desaturated metabolites in our microsomal incubations, combined with the oxygenated metabolites described above, demonstrates the efficacy of in vitro biosynthesis as a tool for generating a large and structurally diverse set of metabolites. Experimental MS/MS fragmentation spectra of the parent QACs and QAC metabolites can be downloaded as a database file on GitHub (https://github.com/libinxulab/xulab_software.git).

IM-MS Analysis of Human Liver Microsome QAC Incubations. We analyzed each HLM reaction mixture via LC-IM-MS/MS. $^{TWIM}CCS_{N_2}$ values were calibrated using a series of singly charged poly-DL-alanines ($n = 2-14$), a custom mixture of drug and drug-like compounds ($n = 7$), and a mixture of HFAPs from the Agilent ESI-L low-concentration tuning mix ($n = 4$) as previously described.^{29,30} To assess the reference $^{TWIM}CCS_{N_2}$ values reported herein, we compared our data to previously published literature values^{8,29,30} (Table S2 and Figure 5).

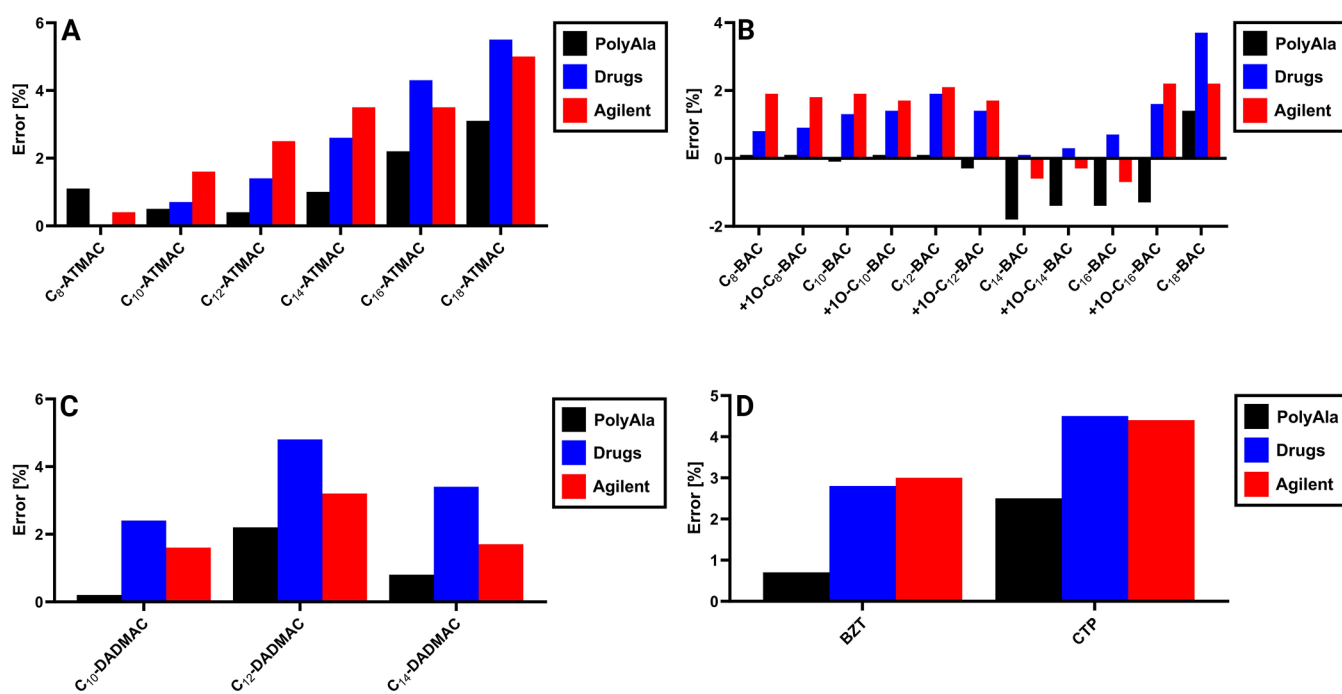


Figure 5. Comparison of measured $^{TWIM}CCS_{N_2}$ values with published literature values.^{8,29,30} Calculated percentage errors from each set of CCS calibrants for (A) parent ATMAs, (B) parent BACs and selected BAC metabolites, (C) DADMACs, and (D) BZT and CTP. For a complete list of measured percentage errors (PEs), see Table S2.

For a complete list of experimental $^{TWIM}CCS_{N_2}$ values obtained in this study, see the [Supporting Information](#). Compared to the $^{DT}CCS_{N_2}$ values recently reported by Belova et al.,⁸ the observed absolute percentage errors (APEs) for our reported $^{TWIM}CCS_{N_2}$ values ranged from 0.02% (C₈-ATMAC, drug mixture calibration) to 5.5% (C₁₈-ATMAC, drug mixture calibration). Belova et al.⁸ reported an increase in the observed APEs of BACs as the alkyl chain lengths increased, which was attributed to differences in the correlation trends between the $^{TWIM}CCS_{N_2}$ values and m/z ratios. We have previously used computational modeling to show that for a series of parent BACs (C₄–C₁₆), distributions of the intramolecular distance between the quaternary ammonium nitrogen and the ω -carbon of the alkyl chain generally increase in magnitude and spread with increasing alkyl chain length.²⁹ BACs with longer alkyl chains are therefore more dynamic and exhibit a greater number of gas-phase conformations than short-chain BACs, leading to broader mobiligrams and more inherent variance in the CCS calculations. This trend was generally recapitulated in our reported $^{TWIM}CCS_{N_2}$ data for the ATMAs and BACs investigated across all CCS calibrant sets, with the highest APEs observed for C₁₈-ATMAC. While we did not observe a discernible pattern within the DADMAC series, the relatively high observed APEs for all alkyl chain lengths and CCS calibrants investigated likely reflect the broad mobiligrams of these compounds. These differences could also be explained by our selection of external calibrants, which are known to influence $^{TWIM}CCS_{N_2}$ interplatform reproducibility,³⁶ as well as fundamental differences in ion transport between DTIM and our TWIM platform.⁴⁴ On average, the observed APEs ranged from 1.0% (PolyAla calibration) to 2.2% (Agilent calibration). These values align with interlaboratory deviations reported in the literature.^{36,45} Furthermore, the low APEs (<2.2%) observed for the + O BAC metabolites, in comparison with

our previously reported $^{TWIM}CCS_{N_2}$ data,²⁹ indicate the high reproducibility of these measurements.

Measurements for all 19 parent QACs and their phase I hepatic metabolites included in this study were obtained on multiple occasions ($n = 3$ to 6) over a period of 9 months, with high reproducibility (<2% interday and intraday RSD). A total of 81 NADPH-dependent metabolites were generated from the 19 parent QACs, representing oxidation (+1O and +2O), a combination of oxidation and desaturation (+1O,–2H, +2O,–2H, and +3O,–2H), and desaturation (–2H) modifications (Table 1). Among the 75 observed oxygenated QAC metabolites (+1O, +2O, +1O,–2H, +2O,–2H, and +3O,–2H), 9 metabolites did not meet the extracted mobiligram intensity cutoff (specified in [Materials and Methods](#)) and were excluded from the QAC reference database. The $^{TWIM}CCS_{N_2}$ (PolyAla calibration) vs m/z values for parent QACs and their metabolites are displayed in [Figure 6A](#).

In general, parent QACs displayed a larger CCS than that of their phase I hepatic metabolites. To measure the extent of the structural compaction/expansion of these metabolites relative to that of their corresponding parent compounds, a dimensionless compaction factor (C) was calculated using eq 1, as previously described²⁹

$$\left(\frac{CCS_{\text{parent}}}{CCS_{\text{metabolite}}} \right) = C \times \left(\frac{\text{mass}_{\text{parent}}}{\text{mass}_{\text{metabolite}}} \right)^{2/3} \quad (1)$$

Here, a value of $C < 1$ indicates that the metabolite becomes less compact than the parent, while a value of $C > 1$ indicates that the metabolite becomes more compact than the parent. Remarkably, despite their increased mass, each of the + O metabolites in the ATMAC series (C₈–C₁₆) displayed a consistent linear decrease in CCS compared to their respective parent compounds ([Figure 6B](#)). Furthermore, the compaction factors for these metabolites were greater than 1, and the

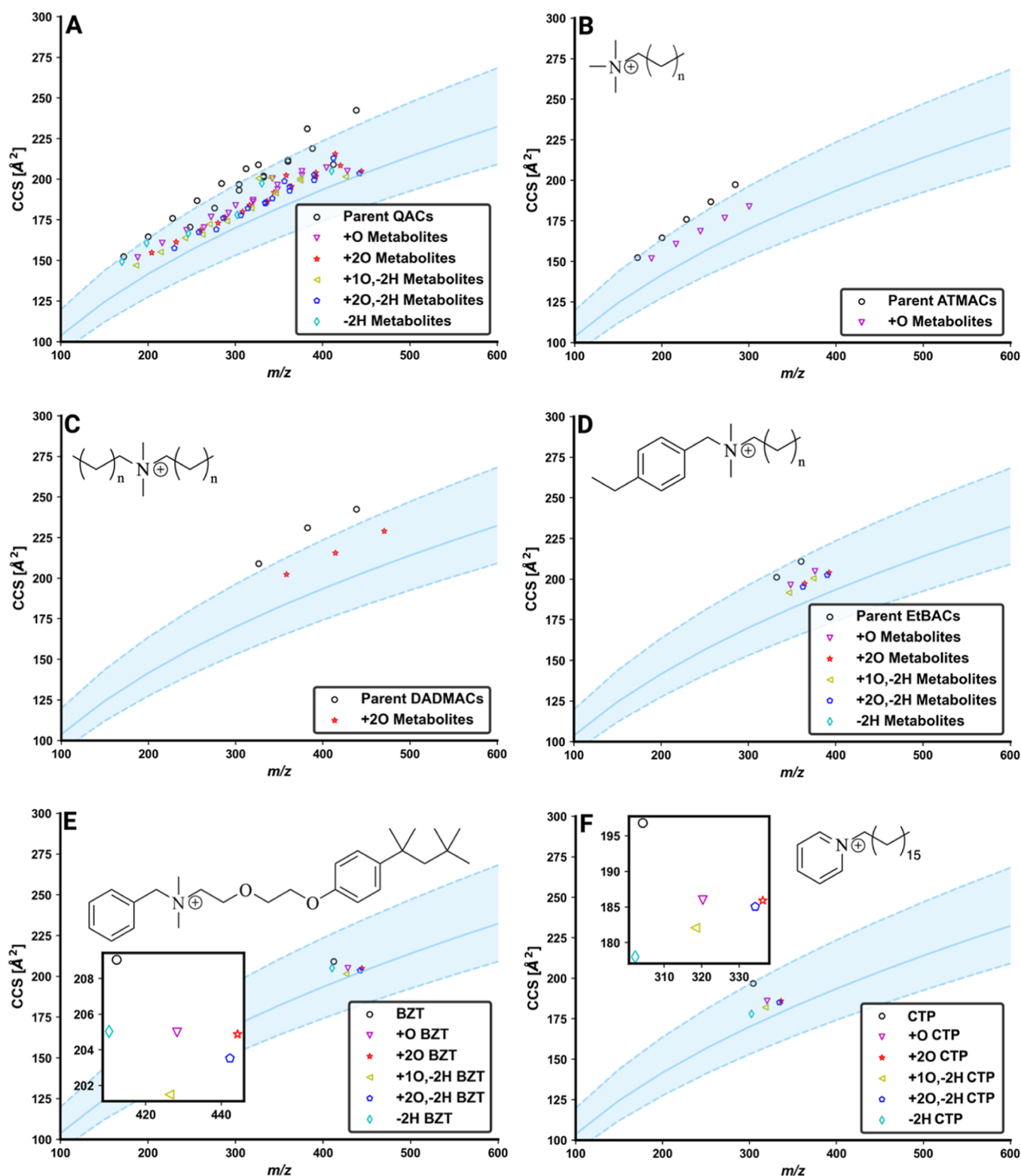


Figure 6. IM-MS conformational space plots. (A) Measured $^{TWIM}CCS_{N_2}$ (PolyAla calibration) vs m/z values for (A) all 19 parent QACs and their 75 observed phase I hepatic metabolites (excluding +3O-2H metabolites), (B) ATMACs (C_8 – C_{16}) and +1O metabolites, (C) DADMACs (C_{10} – C_{14}) and +2O metabolites, (D) EtBACs (C_{12} and C_{14}) and observed phase I hepatic metabolites, (E) BZT and observed phase I hepatic metabolites, and (F) CTP and observed phase I hepatic metabolites.

degree of compaction increased with the lengthening of the alkyl chain (Table S3). This trend was also generally observed within the series of +2O-DADMAC metabolites (Figure 6C) and for all oxygenated metabolites of C_{12} - and C_{14} -EtBAC (Figure 6D). We have previously reported that BACs exhibit

similar yet unusual CCS behavior upon CYP-mediated ω -hydroxylation.²⁹ Strong intramolecular ion–dipole interactions are formed between the positively charged quaternary ammonium center and the oxygen atom at the opposite end of the metabolite. These interactions effectively restrict the

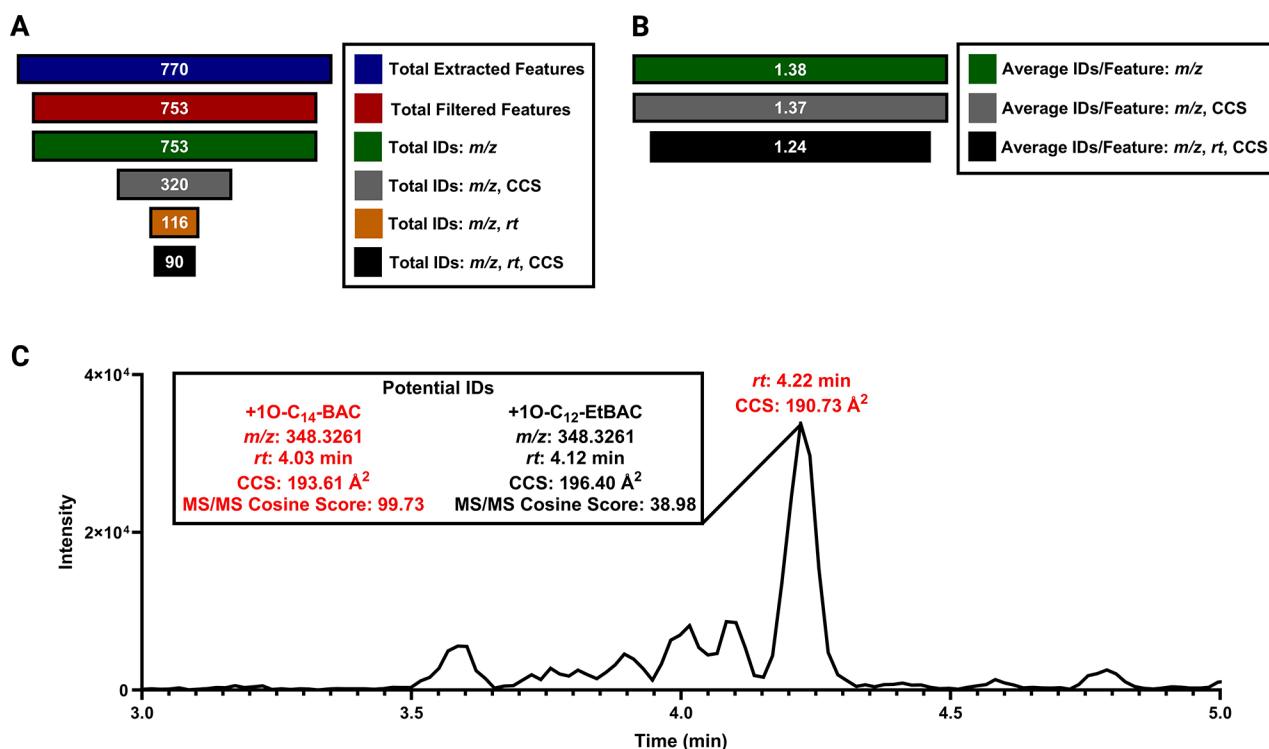


Figure 7. Application of the QAC and metabolite reference database. (A) Total number of extracted and filtered spectral features from the pooled human fecal extract, as well as total number of compound identifications with varying levels of selection criteria. (B) Average number of compound identifications per spectral feature with varying levels of selection criteria. (C) Extracted m/z -selected LC ion chromatogram (348.3261 ± 0.025 Da) demonstrating the use of MS/MS cosine similarity scoring for ranking potential compound identifications at the m/z , CCS, and rt selection criteria level.

dynamics of the alkyl chain, thereby promoting structural compaction. On average, the C values of the +O ATMAC metabolites were 2.6% higher than those of the ω -OH BAC metabolites with equal alkyl chain length, indicating an increased degree of compaction in ATMACs compared to BACs following hydroxylation. This observation could be explained by the substitution of a benzyl moiety with a less bulky methyl group on the ATMAC structure, which likely reduces interactions with the drift gas.

Similarly, the +O metabolites of BZT (Figure 6E) and CTP (Figure 6F) displayed CCS values that were smaller than those of their respective parent compounds, indicating structural compaction. The degree of compaction was greater in the +O metabolites of CTP ($C = 1.10$) compared to the +O metabolites of BZT ($C = 1.05$), which suggests that the conformational changes induced by hydroxylation are influenced by the structure of the parent compound. Furthermore, the +2O, +1O, -2H, and +2O, -2H metabolites of BZT and CTP all displayed C values greater than 1. The extent of compaction, however, was more pronounced in the desaturated (-2H) metabolite of CTP ($C = 1.10$) compared to the desaturated metabolite of BZT ($C = 1.02$). This observation could be attributed to the putative formation of a double bond along the alkyl chain region of CTP and the TMP moiety of BZT. The presence of such a double bond would introduce an electron- π system within the molecule, leading to electrostatic interactions with the positively charged quaternary ammonium center. These findings highlight the complex and distinct gas-phase conformational changes induced by different metabolic routes.

LC-IM-MS/MS Analysis of Human Fecal Samples. To demonstrate the utility of our QAC reference database, we first analyzed a pooled human fecal extract derived from five fecal samples (two samples from the same individual and three samples from three other individuals) using LC-IM-MS/MS (see LC-IM-MS/MS Analysis of Human Fecal Samples). Several recent studies support the suitability of feces for the biomonitoring of QACs and QAC metabolites. As shown by Luz et al., orally administered ¹⁴C-radiolabeled BACs (C_{12} , C_{14} , and C_{16}) and C_{10} -DADMAC in rats led to 88–98% recovery of radioactivity in feces, with approximately one-third of BACs and one-half of C_{10} -DADMAC recovered as oxidized metabolites.⁴⁶ In the same study, rats given a single IV dose of ¹⁴C-radiolabeled BACs excreted 45–55% of radioactivity to feces, with 20–30% excreted to urine and 30–35% remaining in tissues at 7 days post-administration, suggesting that feces is a major excretion route regardless of the exposure routes. While ω -hydroxy and ω -carboxylic acid BAC metabolites have been detected in human urine and serum,⁴⁷ parent BACs are not typically found in urine and QAC metabolite levels in serum are relatively low (0.03–0.04 ng/mL for +10- C_8 -BAC and 0.01 ng/mL for +2O, -2H- C_{10} -BAC). Fecal samples are, therefore, logical for the simultaneous detection of parent QACs and QAC metabolites. Additionally, the highly complex and heterogeneous composition of feces provides an excellent opportunity to demonstrate the advantages of IM-MS-based analytical platforms.

A target list containing the exact m/z values of all parent QACs and their observed phase I hepatic metabolites (96 total entries) was compiled and used to automatically process the raw data files. This workflow generated a list of extracted

spectral features, which was compared against the spectral features extracted from a gradient-matched blank water control to remove non-unique entries. As shown in Figure 7A, the filtering step removed 17 non-unique spectral features from the list, and the remaining extracted spectral features were queried against the QAC reference database with various selection criteria (m/z tolerance: 0.025 Da; rt tolerance: 0.2 min; CCS tolerance: 3%). The total number of annotated spectral features was reduced from 753 to 320 with the inclusion of the CCS, suggesting that drift time filters can be used to efficiently remove false positives. IM separation proved to be a valuable tool for reducing the number of putative annotations for coeluting analytes with identical m/z values. For example, distinguishing between the isobaric, coeluting +3O,−2H metabolites of C₁₄-BAC and C₁₂-EtBAC was only possible by leveraging the CCS values of these compounds (Figure S13). Furthermore, the inclusion of rt reduced both the total number of annotated spectral features from 320 to 90 and the average number of annotations per feature from 1.38 to 1.24 (Figure 7B). These results suggest that the tandem use of m/z , CCS, and rt criteria improves the confidence of compound detection in complex biological matrices by reducing the average number of annotations per spectral feature. The decrease in total annotations also reduces the occurrence of false positives and thus could facilitate downstream analysis of large-scale human biomonitoring studies.

Out of the 90 spectral features with matches based on the m/z , CCS, and rt criteria, we identified a total of 13 unique parent QACs and at least one compound from each subclass represented in the reference database (i.e., ATMACs, BACs, EtBACs, DADMACs, BZT, and CTP) (Figure S14). Using the extracted retention and drift times for each annotated spectral feature, we also extracted rt - and dt -selected post-IM fragmentation spectra from the pooled human fecal extract raw file to calculate MS/MS cosine similarity scores with previously collected reference spectra (see LC-IM-MS/MS Analysis of Human Fecal Samples).

Cosine similarity is a well-established metric in the field of mass spectrometry.^{48,49} This method quantifies the similarity between two mass spectra by calculating the dot product of their respective vectors, which are constructed from m/z values and the corresponding intensity levels. The cosine similarity score between two mass spectra can range from 0 to 100, with higher values denoting greater similarity. As shown in Figures S14 and S15, we obtained similar MS/MS cosine similarity scores for the detected parent QACs and QAC metabolites using experimental (i.e., previously collected on the same instrument) and theoretical (i.e., *in silico*) reference fragmentation spectra. These results indicate that when samples and reference mixtures are analyzed on the same instrument, both experimental and theoretical fragmentation spectra are appropriate for constructing reference databases.

We identified a total of 35 QAC metabolites with matches based on the m/z , CCS, and rt criteria in the pooled human fecal extract, including monohydroxylated (+1O) and further oxidized (+1O,−2H, +2O,−2H, and +3O,−2H) metabolites for each QAC subclass. Dihydroxylated (+2O) ATMAC, BAC, and DADMAC metabolites were also identified. Collectively, these findings indicate that IM analysis can be used to profile the exposure of both hydrophobic parent compounds and their polar metabolites in a complex biological matrix. The utilization of MS/MS cosine similarity scoring was particularly useful for increasing the confidence of QAC metabolite

annotations with identical m/z values. As shown in Figure 7C, the +1O metabolites of C₁₄-BAC and C₁₂-EtBAC are constitutional isomers with similar measured CCS values and retention times. Applying the selection criteria described above (m/z tolerance: 0.025 Da; rt tolerance: 0.2 min; CCS tolerance: 3%), the spectral feature identified in the pooled human fecal extract at 4.22 min and 190.73 Å² was ambiguously annotated as both +1O-C₁₄-BAC and +1O-C₁₂-EtBAC, two structurally distinct QAC metabolites with identical molecular formulas. The inclusion of MS/MS cosine similarity scoring, however, enabled the clear assignment of +1O-C₁₄-BAC to this spectral feature given its significantly higher similarity to the metabolite's reference fragmentation spectrum. Taken together, these data indicate that MS/MS cosine similarity is a valuable tool for ranking the putative annotations of spectral features with multiple compound matches.

To further investigate the distribution of QACs in human feces, we analyzed the 5 individual fecal samples via LC-IM-MS/MS. Using the selection criteria described above, we detected a total of 14 unique parent QACs across the 5 samples, including all 13 compounds originally identified in the pooled extract with the addition of C₁₀-BAC (Figure S16). The Supporting Information summarizes all extracted and filtered spectral features and identifications from these samples. The lack of detection of C₁₀-BAC in the pooled extract could be due to the effective 5-fold dilution when the samples were combined, which potentially lowered the compound's concentration below the detection limit of the instrument. Out of the 13 parent QACs, 5 compounds (C₁₂-ATMAC, C₁₂-BAC, C₁₄-BAC, C₁₆-BAC, and C₁₀-DADMAC) were identified in all 5 samples and 4 compounds (C₁₈-ATMAC, C₁₂-EtBAC, C₁₄-EtBAC, and CTP) were identified in 80% (4 out of 5) of the samples. Notably, we did not observe short-chain ATMACs (C₈–C₁₀) or C₈-BAC in any of the human fecal samples, which could potentially be explained by their relatively lower abundance in commercial products,¹ lower bioaccumulation potential,¹ and/or decreased metabolic stability relative to those of longer-chain QACs.²⁸ To assess the reproducibility of our method, we independently analyzed two aliquots of human feces derived from a single sample from the same donor (samples 1A,B in Figure S16). A total of 13 unique parent QACs were identified in the first replicate. Of these, 12 were also present in the second replicate; the only exception was BZT, which is likely explained by its low abundance in the fecal sample. This consistency indicates the high reproducibility of our experimental workflow.

Using *d*₇-labeled internal standards, BAC (C₁₀–C₁₆) concentrations were semiquantified in the human fecal samples (Figure S17 and Table S4). The relative abundance of each BAC was strikingly similar across the 3 fecal samples that contained all 4 identified compounds in the following order, C₁₀ < C₁₆ < C₁₂ < C₁₄ (samples 1A,B, and 2 in Figure S17). Notably, C₁₀-BAC was not detected based on m/z , CCS, and rt selection criteria in 2 of the fecal samples. These results are consistent with the relative abundances of BACs in many commercial products that contain a mixture of BACs with varying alkyl chain lengths.¹ The BACs with the highest relative abundance in all 5 fecal samples were C₁₂ and C₁₄. Because these two BAC compounds have the highest biocidal activity,⁵⁰ they typically represent the greatest proportion within commercial mixtures. The median BAC levels in feces reported herein are significantly higher (>10-fold) than median

blood levels for each alkyl chain length.¹² The relatively large quantity of BACs in feces could reflect the use of BACs in food-processing settings and subsequent oral intake. If BAC exposure occurs by inhalation, possible explanations include relatively brief plasma half-lives (1.8–3.7 h for C₁₂, C₁₄, and C₁₆ BAC in rats)⁵¹ and/or formation of BAC–bile acid ion pair complexes⁵² that undergo P-glycoprotein efflux transport at the bile canalicular membrane of hepatocytes and ultimately deposit into the intestinal lumen. Additional studies, however, are required to further characterize the various transport and excretion pathways involved in the QAC disposition.

Collectively, our results indicate that QACs and many of their phase I hepatic metabolites are detectable in human feces and that these compounds can be confidently assigned to spectral features with the tandem utilization of CCS, *rt*, and MS/MS fragmentation reference databases in biomonitoring efforts. The experimental workflow and data processing tools developed in this study may be applied to other classes of environmental contaminants and in vitro-generated metabolites.

■ ASSOCIATED CONTENT

SI Supporting Information

The Supporting Information is available free of charge at <https://pubs.acs.org/doi/10.1021/acs.est.3c10845>.

MS/MS fragmentation spectra of parent QACs and their metabolites, comparison of measured ^{TWIM}CCS_{N₂} values with literature values, compaction factors of selected QAC metabolites, MS/MS cosine similarity scores, distribution of QAC and QAC metabolites in human fecal samples, and semiquantified BAC concentrations in human fecal samples (PDF)

Measured ^{TWIM}CCS_{N₂} for QACs and QAC metabolites with relative standard deviations, mass accuracies, retention times, and characteristic fragmentation data (XLSX)

Summary of all extracted and filtered spectral features from 5 human fecal samples, compound identifications based on (1) *m/z*, (2) *m/z* and CCS, and (3) *m/z*, CCS, and *rt*, and compound rankings based on MS/MS cosine similarity scoring with experimental and theoretical fragmentation databases (XLSX)

■ AUTHOR INFORMATION

Corresponding Author

Libin Xu – Department of Medicinal Chemistry, University of Washington, Seattle, Washington 98195, United States; orcid.org/0000-0003-1021-5200; Phone: (206) 543-1080; Email: libinxu@uw.edu; Fax: (206) 685-3252

Authors

Ryan Nguyen – Department of Medicinal Chemistry, University of Washington, Seattle, Washington 98195, United States

Ryan P. Seguin – Department of Medicinal Chemistry, University of Washington, Seattle, Washington 98195, United States

Dylan H. Ross – Department of Medicinal Chemistry, University of Washington, Seattle, Washington 98195, United States; Present Address: Biological Sciences Division, Pacific Northwest National Laboratory, Richland, WA 99352, United States; orcid.org/0009-0005-2943-2282

Pengyu Chen – Department of Medicinal Chemistry, University of Washington, Seattle, Washington 98195, United States

Sean Richardson – Department of Mathematics, University of Washington, Seattle, Washington 98195, United States

Jennifer Liem – Department of Pharmaceutics, University of Washington, Seattle, Washington 98195, United States

Yvonne S. Lin – Department of Pharmaceutics, University of Washington, Seattle, Washington 98195, United States

Complete contact information is available at:

<https://pubs.acs.org/10.1021/acs.est.3c10845>

Author Contributions

L.X. conceptualized and supervised the study; R.N., R.P.S., D.H.R., J.L., Y.S.L., and L.X. participated in experimental design; R.N., R.P.S., and D.H.R. conducted experiments; R.N. performed data analysis; S.R. contributed to the writing of the Python code; P.C. contributed to the design of the web interface for the database; R.N. contributed to the writing of the original draft; R.N., R.P.S., J.L., Y.S.L., and L.X. contributed to the review and editing of the manuscript.

Notes

The authors declare no competing financial interest.

■ ACKNOWLEDGMENTS

The authors would like to thank the University of Washington School of Pharmacy Mass Spectrometry Center for instrument support. This work was funded by a National Institutes of Health Grant (R01ES031927 to L.X.) and the Environmental Pathology and Toxicology Training Grant (National Institutes of Environmental Health Sciences T32ES007032 to R.N.).

■ REFERENCES

- (1) Arnold, W. A.; Blum, A.; Branyan, J.; Bruton, T. A.; Carignan, C. C.; Cortopassi, G.; Datta, S.; DeWitt, J.; Doherty, A.-C.; Halden, R. U.; Harari, H.; Hartmann, E. M.; Hrubec, T. C.; Iyer, S.; Kwiatkowski, C. F.; LaPier, J.; Li, D.; Li, L.; Muñoz Ortiz, J. G.; Salamova, A.; Schettler, T.; Seguin, R. P.; Soehl, A.; Sutton, R.; Xu, L.; Zheng, G. Quaternary Ammonium Compounds: A Chemical Class of Emerging Concern. *Environ. Sci. Technol.* **2023**, *57*, 7645–7665.
- (2) Pati, S. G.; Arnold, W. A. Comprehensive Screening of Quaternary Ammonium Surfactants and Ionic Liquids in Wastewater Effluents and Lake Sediments. *Environ. Sci. Process. Impacts* **2020**, *22* (2), 430–441.
- (3) Hora, P. I.; Pati, S. G.; McNamara, P. J.; Arnold, W. A. Increased Use of Quaternary Ammonium Compounds during the SARS-CoV-2 Pandemic and Beyond: Consideration of Environmental Implications. *Environ. Sci. Technol. Lett.* **2020**, *7* (9), 622–631.
- (4) Mohapatra, S.; Yutao, L.; Goh, S. G.; Ng, C.; Luhua, Y.; Tran, N. H.; Gin, K. Y.-H. Quaternary Ammonium Compounds of Emerging Concern: Classification, Occurrence, Fate, Toxicity and Antimicrobial Resistance. *J. Hazard. Mater.* **2023**, *445*, 130393.
- (5) Martínez-Carballo, E.; González-Barreiro, C.; Sitka, A.; Kreuzinger, N.; Scharf, S.; Gans, O. Determination of Selected Quaternary Ammonium Compounds by Liquid Chromatography with Mass Spectrometry. Part II. Application to Sediment and Sludge Samples in Austria. *Environ. Pollut.* **2007**, *146* (2), 543–547.
- (6) Ruan, T.; Song, S.; Wang, T.; Liu, R.; Lin, Y.; Jiang, G. Identification and Composition of Emerging Quaternary Ammonium Compounds in Municipal Sewage Sludge in China. *Environ. Sci. Technol.* **2014**, *48* (8), 4289–4297.
- (7) Zheng, G.; Filippelli, G. M.; Salamova, A. Increased Indoor Exposure to Commonly Used Disinfectants during the COVID-19 Pandemic. *Environ. Sci. Technol. Lett.* **2020**, *7* (10), 760–765.

- (8) Belova, L.; Poma, G.; Roggeman, M.; Jeong, Y.; Kim, D.-H.; Berghmans, P.; Peters, J.; Salamova, A.; van Nuijs, A. L. N.; Covaci, A. Identification and Characterization of Quaternary Ammonium Compounds in Flemish Indoor Dust by Ion-Mobility High-Resolution Mass Spectrometry. *Environ. Int.* **2023**, *177*, 108021.
- (9) Takeoka, G. R.; Dao, L. T.; Wong, R. Y.; Harden, L. A. Identification of Benzalkonium Chloride in Commercial Grapefruit Seed Extracts. *J. Agric. Food Chem.* **2005**, *53* (19), 7630–7636.
- (10) Kröckel, L.; Jira, W.; Wild, D. Identification of Benzalkonium Chloride in Food Additives and Its Inefficacy against Bacteria in Minced Meat and Raw Sausage Batters. *Eur. Food Res. Technol.* **2003**, *216* (5), 402–406.
- (11) Slimani, K.; Feret, A.; Pirotais, Y.; Maris, P.; Abjean, J. P.; Hurtaud-Pessel, D. Liquid Chromatography-Tandem Mass Spectrometry Multiresidue Method for the Analysis of Quaternary Ammonium Compounds in Cheese and Milk Products: Development and Validation Using the Total Error Approach. *J. Chromatogr A* **2017**, *1517*, 86–96.
- (12) Hrubec, T. C.; Seguin, R. P.; Xu, L.; Cortopassi, G. A.; Datta, S.; Hanlon, A. L.; Lozano, A. J.; McDonald, V. A.; Healy, C. A.; Anderson, T. C.; Musse, N. A.; Williams, R. T. Altered Toxicological Endpoints in Humans from Common Quaternary Ammonium Compound Disinfectant Exposure. *Toxicol Rep* **2021**, *8*, 646–656.
- (13) Zheng, G.; Webster, T. F.; Salamova, A. Quaternary Ammonium Compounds: Bioaccumulation Potentials in Humans and Levels in Blood before and during the Covid-19 Pandemic. *Environ. Sci. Technol.* **2021**, *55* (21), 14689–14698.
- (14) Zheng, G.; Schreder, E.; Sathyarayanan, S.; Salamova, A. The First Detection of Quaternary Ammonium Compounds in Breast Milk: Implications for Early-Life Exposure. *J. Expo. Sci. Environ. Epidemiol.* **2022**, *32* (5), 682–688.
- (15) US FDA Safety and Effectiveness of Health Care Antiseptics; Topical Antimicrobial Drug Products for Over-the-Counter Human Use; Proposed Amendment of the Tentative Final Monograph; Reopening of Administrative Record. *Fed. Regist.*, 2015; Vol. 21 CFR Part 310, 80, pp 25165–25205.
- (16) US FDA Safety and Effectiveness of Consumer Antiseptics; Topical Antimicrobial Drug Products for Over-the-Counter Human Use; Proposed Amendment of the Tentative Final Monograph; Reopening of Administrative Record. *Fed. Regist.*, 2016; Vol. 21 CFR Part 310, 81, pp 42911–42937.
- (17) Quaternary Ammonium Compounds. <https://www.mass.gov/doc/draft-quaternary-ammonium-compounds-policy-analysis-july-12-2022/download> (accessed Sept 7, 2023).
- (18) Datta, S.; He, G.; Tomilov, A.; Sahdeo, S.; Denison, M. S.; Cortopassi, G. In Vitro Evaluation of Mitochondrial Function and Estrogen Signaling in Cell Lines Exposed to the Antiseptic Cetylpyridinium Chloride. *Env. Health Perspect* **2017**, *125* (8), 087015.
- (19) Datta, S.; Baudouin, C.; Brignole-Baudouin, F.; Denoyer, A.; Cortopassi, G. A. The Eye Drop Preservative Benzalkonium Chloride Potently Induces Mitochondrial Dysfunction and Preferentially Affects LHON Mutant Cells. *Invest Ophthalmol Vis Sci.* **2017**, *58* (4), 2406–2412.
- (20) Herron, J.; Reese, R.; Tallman, K. A.; Narayanaswamy, R.; Porter, N. A.; Xu, L. Identification of Environmental Quaternary Ammonium Compounds as Direct Inhibitors of Cholesterol Biosynthesis. *Toxicol. Sci.* **2016**, *151* (2), 261–270.
- (21) van Wijk, D.; Gyimesi-van den Bos, M.; Garttner-Arends, I.; Geurts, M.; Kamstra, J.; Thomas, P. Bioavailability and Detoxification of Cationics: I. Algal Toxicity of Alkyltrimethyl Ammonium Salts in the Presence of Suspended Sediment and Humic Acid. *Chemosphere* **2009**, *75* (3), 303–309.
- (22) Isomaa, B.; Bjondahl, K. Toxicity and Pharmacological Properties of Surface-Active Alkyltrimethylammonium Bromides in the Rat. *Acta Pharmacol. Toxicol.* **1980**, *47* (1), 17–23.
- (23) Larsen, S. T.; Verder, H.; Nielsen, G. D. Airway Effects of Inhaled Quaternary Ammonium Compounds in Mice. *Basic Clin. Pharmacol. Toxicol.* **2012**, *110* (6), 537–543.
- (24) Melin, V. E.; Potineni, H.; Hunt, P.; Griswold, J.; Siems, B.; Werre, S. R.; Hrubec, T. C. Exposure to Common Quaternary Ammonium Disinfectants Decreases Fertility in Mice. *Reprod. Toxicol.* **2014**, *50*, 163–170.
- (25) Isaac, J.; Scheinman, P. L. Benzalkonium Chloride: An Irritant and Sensitizer. *Dermat. Contact Atopic Occup. Drug* **2017**, *28* (6), 346–352.
- (26) Bellier, M.; Barnig, C.; Renaudin, J. M.; Sbinne, B.; Lefebvre, F.; Qi, S.; de Blay, F. Importance of Specific Inhalation Challenge in the Diagnosis of Occupational Asthma Induced by Quaternary Ammonium Compounds. *J. Allergy Clin Immunol Pr.* **2015**, *3* (5), 819–820.
- (27) Dumas, O.; Varraso, R.; Boggs, K. M.; Quinot, C.; Zock, J.-P.; Henneberger, P. K.; Speizer, F. E.; Le Moual, N.; Camargo, C. A. Association of Occupational Exposure to Disinfectants With Incidence of Chronic Obstructive Pulmonary Disease Among US Female Nurses. *JAMA Netw. Open* **2019**, *2* (10), No. e1913563.
- (28) Seguin, R. P.; Herron, J. M.; Lopez, V.; Dempsey, J. L.; Xu, L. Metabolism of Benzalkonium Chlorides by Human Hepatic Cytochromes P450. *Chem. Res. Toxicol.* **2019**, *32* (12), 2466–2478.
- (29) Ross, D. H.; Seguin, R. P.; Xu, L. Characterization of the Impact of Drug Metabolism on the Gas-Phase Structures of Drugs Using Ion Mobility-Mass Spectrometry. *Anal. Chem.* **2019**, *91* (22), 14498–14507.
- (30) Hines, K. M.; Ross, D. H.; Davidson, K. L.; Bush, M. F.; Xu, L. Large-Scale Structural Characterization of Drug and Drug-Like Compounds by High-Throughput Ion Mobility-Mass Spectrometry. *Anal. Chem.* **2017**, *89*, 9023–9030.
- (31) Hernández-Mesa, M.; D'Atri, V.; Barknowitz, G.; Fanuel, M.; Pezzatti, J.; Dreolin, N.; Ropartz, D.; Monteau, F.; Vigneau, E.; Rudaz, S.; Stead, S.; Rogniaux, H.; Guillaume, D.; Dervilly, G.; Le Bizec, B. Interlaboratory and Interplatform Study of Steroids Collision Cross Section by Traveling Wave Ion Mobility Spectrometry. *Anal. Chem.* **2020**, *92* (7), 5013–5022.
- (32) Righetti, L.; Dreolin, N.; Celma, A.; McCullagh, M.; Barknowitz, G.; Sancho, J. V.; Dall'Asta, C. Travelling Wave Ion Mobility-Derived Collision Cross Section for Mycotoxins: Investigating Interlaboratory and Interplatform Reproducibility. *J. Agric. Food Chem.* **2020**, *68* (39), 10937–10943.
- (33) Ross, D. H.; Cho, J. H.; Xu, L. Breaking Down Structural Diversity for Comprehensive Prediction of Ion-Neutral Collision Cross Sections. *Anal. Chem.* **2020**, *92* (6), 4548–4557.
- (34) Belova, L.; Celma, A.; Van Haesendonck, G.; Lemièrre, F.; Sancho, J. V.; Covaci, A.; van Nuijs, A. L. N.; Bijlsma, L. Revealing the Differences in Collision Cross Section Values of Small Organic Molecules Acquired by Different Instrumental Designs and Prediction Models. *Anal. Chim. Acta* **2022**, *1229*, 340361.
- (35) Ross, D. H.; Seguin, R. P.; Krinsky, A. M.; Xu, L. High-Throughput Measurement and Machine Learning-Based Prediction of Collision Cross Sections for Drugs and Drug Metabolites. *J. Am. Soc. Mass Spectrom.* **2022**, *33*, 1061–1072.
- (36) Hines, K. M.; May, J. C.; McLean, J. A.; Xu, L. Evaluation of Collision Cross Section Calibrants for Structural Analysis of Lipids by Traveling Wave Ion Mobility-Mass Spectrometry. *Anal. Chem.* **2016**, *88* (14), 7329–7336.
- (37) *scipy.signal.find_peaks* — SciPy v1.11.2 Manual. https://docs.scipy.org/doc/scipy/reference/generated/scipy.signal.find_peaks.html (accessed Sept 11, 2023).
- (38) Tsugawa, H.; Kind, T.; Nakabayashi, R.; Yukihiro, D.; Tanaka, W.; Cajka, T.; Saito, K.; Fiehn, O.; Arita, M. Hydrogen Rearrangement Rules: Computational MS/MS Fragmentation and Structure Elucidation Using MS-FINDER Software. *Anal. Chem.* **2016**, *88* (16), 7946–7958.
- (39) Ross, D. H.; Cho, J. H.; Zhang, R.; Hines, K. M.; Xu, L. Lipidomics: A Python Package for Comprehensive Prediction of Lipid Collision Cross Sections and Retention Times and Analysis of Ion Mobility-Mass Spectrometry-Based Lipidomics Data. *Anal. Chem.* **2020**, *92* (22), 14967–14975.

- (40) Malm, L.; Palm, E.; Souihi, A.; Plassmann, M.; Liigand, J.; Krueve, A. Guide to Semi-Quantitative Non-Targeted Screening Using LC/ESI/HRMS. *Mol. Basel Switz.* **2021**, *26* (12), 3524.
- (41) Attia, S. M. Deleterious Effects of Reactive Metabolites. *Oxid. Med. Cell. Longev.* **2010**, *3* (4), 238–253.
- (42) Ley, S. V. *The Practice of Medicinal Chemistry*; Elsevier, 2003.
- (43) Rettie, A. E.; Boberg, M.; Rettenmeier, A. W.; Baillie, T. A. Cytochrome P-450-Catalyzed Desaturation of Valproic Acid in Vitro. Species Differences, Induction Effects, and Mechanistic Studies. *J. Biol. Chem.* **1988**, *263* (27), 13733–13738.
- (44) Feuerstein, M. L.; Hernández-Mesa, M.; Valadbeigi, Y.; Le Bizec, B.; Hann, S.; Dervilly, G.; Causon, T. Critical Evaluation of the Role of External Calibration Strategies for IM-MS. *Anal. Bioanal. Chem.* **2022**, *414* (25), 7483–7493.
- (45) Hinnenkamp, V.; Klein, J.; Meckelmann, S. W.; Balsaa, P.; Schmidt, T. C.; Schmitz, O. J. Comparison of CCS Values Determined by Traveling Wave Ion Mobility Mass Spectrometry and Drift Tube Ion Mobility Mass Spectrometry. *Anal. Chem.* **2018**, *90* (20), 12042–12050.
- (46) Luz, A.; DeLeo, P.; Pechacek, N.; Freemantle, M. Human Health Hazard Assessment of Quaternary Ammonium Compounds: Didecyl Dimethyl Ammonium Chloride and Alkyl (C12-C16) Dimethyl Benzyl Ammonium Chloride. *Regul. Toxicol. Pharmacol.* **2020**, *116*, 104717.
- (47) Kelly, P. E.; Ng, H. J.; Farrell, G.; McKirdy, S.; Russell, R. K.; Hansen, R.; Rattray, Z.; Gerasimidis, K.; Rattray, N. J. W. An Optimised Monophasic Faecal Extraction Method for LC-MS Analysis and Its Application in Gastrointestinal Disease. *Metabolites* **2022**, *12* (11), 1110.
- (48) Moorthy, A. S.; Kearsley, A. J. Pattern Similarity Measures Applied to Mass Spectra. In *Progress in Industrial Mathematics: Success Stories*; Cruz, M., Parés, C., Quintela, P., Eds.; SEMA SIMAI Springer Series; Springer International Publishing: Cham, 2021; Vol. 5, pp 43–53.
- (49) Harwood, T. V.; Treen, D. G. C.; Wang, M.; de Jong, W.; Northen, T. R.; Bowen, B. P. BLINK Enables Ultrafast Tandem Mass Spectrometry Cosine Similarity Scoring. *Sci. Rep.* **2023**, *13* (1), 13462.
- (50) Vereshchagin, A. N.; Frolov, N. A.; Egorova, K. S.; Seitkalieva, M. M.; Ananikov, V. P. Quaternary Ammonium Compounds (QACs) and Ionic Liquids (ILs) as Biocides: From Simple Antiseptics to Tunable Antimicrobials. *Int. J. Mol. Sci.* **2021**, *22* (13), 6793.
- (51) Kera, H.; Fuke, C.; Usumoto, Y.; Nasu, A.; Maeda, K.; Mukai, M.; Sato, W.; Tanabe, M.; Kuninaka, H.; Ihama, Y. Kinetics and Distribution of Benzalkonium Compounds with Different Alkyl Chain Length Following Intravenous Administration in Rats. *Leg. Med. Tokyo Jpn.* **2021**, *48*, 101821.
- (52) Song, I. S.; Choi, M. K.; Jin, Q. R.; Shim, W. S.; Shim, C. K. Increased Affinity to Canalicular P-Gp via Formation of Lipophilic Ion-Pair Complexes with Endogenous Bile Salts Is Associated with Mw Threshold in Hepatobiliary Excretion of Quaternary Ammonium Compounds. *Pharm. Res.* **2010**, *27* (5), 823–831.